Microstructured Magnetic Materials for RF Flux Guides in Magnetic Resonance Imaging

M. C. K. Wiltshire,[1*] J. B. Pendry,[2] I. R. Young,[3] D. J. Larkman,[3] D. J. Gilderdale,[3] J. V. Hajnal[3]

Magnetic resonance imaging and spectroscopy systems use coils, either singly or as arrays, to intercept radio-frequency (RF) magnetic flux from regions of interest, often deep within the body. Here, we show that a new magnetic material offers novel possibilities for guiding RF flux to the receiver coil, permitting a clear image to be obtained where none might otherwise be detectable. The new material contains microstructure designed according to concepts taken from the field of photonic band gap materials. In the RF range, it has a magnetic permeability that can be produced to specification while exhibiting negligible direct-current magnetism. The latter property is vital to avoid perturbing the static and audio-frequency magnetic fields needed to obtain image and spectral data. The concept offers a new paradigm for the manipulation of RF flux in all nuclear magnetic resonance systems.

Microstructured materials (μSMs) can manipulate electromagnetic radiation; it is well known that the iridescence of butterfly wings (*1*) is due to the microstructure of their scales. The concept of the photonic band gap (PBG) was introduced in 1987 by Yablonovitch (*2*) and John (*3*). A PBG arises when diffraction by the periodic microstructure is such as to prevent radiation of a certain frequency band from propagating through the material in any direction. Following the theoretical investigations of Ho *et al.* (*4*), Yablonovitch *et al.* (*5*) demonstrated a practical material with a full PBG in the microwave region. Since that time, there has been a burgeoning interest in photonic or electromagnetic crystals, which are μSMs that have full or partial PBGs.

More recently, a different class of microstructure has been proposed in which the structure is on a scale much smaller than the wavelength of radiation, so that the properties can be described by an effective electric permittivity ε and magnetic permeability μ. Previously inaccessible values of ε and μ can be produced with ease. μSMs can now be designed to have positive or negative values of ε and μ at any desired frequency; this capability opens up new opportunities for system designers. For example, a structure of very fine wires arranged on a three-dimensional (3D) lattice behaves like a metal (*6, 7*), but with the plasma frequency in the microwave region (*8*) rather than in the ultraviolet. This medium gives a negative effective permittivity ($\varepsilon < 0$) in the gigahertz range. Artificial structures can also have magnetic activity. Sievenpiper *et al.* (*9*) have demonstrated a magnetically active surface, and we have proposed a structure with 3D magnetic activity (*10*), that is, an effective magnetic permeability differing from unity. Implementation of a material with a negative effective permeability ($\mu < 0$) has recently been demonstrated (*11*). In the latter case, a combination of negative μ with negative ε was exploited to generate a so-called "left-handed" or "negative refractive index" medium (*11, 12*) in the gigahertz spectrum.

We now describe and characterize a magnetic μSM that is active in the RF range, and we demonstrate a practical application that exploits the unusual properties of the material. It has a resonant permeability slightly above the 21.3-MHz operating frequency of a 0.5-T magnetic resonance imaging (MRI) machine, but is negligibly magnetic in a dc field. Thus, the material can be used in the MRI instrument to control the RF flux without disturbing the dc field or the field gradients. To demonstrate the capability of the material, we present MRI images obtained with a small detector coil that is far removed from the object under investigation, but linked to it through the μSM material.

A μSM consists of a fine structure that is small or comparable to the wavelength of operation. Pendry *et al.* (*10*) described a variety of structures that show magnetism without having any magnetic components; here, we concentrate on the "Swiss roll" structure (Fig. 1). The bulk material is made up of a bundle of rolls, 19 in this work, to give a hexagonal close-packed array (Fig. 1A). Each individual Swiss roll consists of a central cylindrical mandrel of radius r_0 upon which is wound a spiral of N turns of a conductor with an insulating backing, so that there is no electrical contact between the layers, which have a total thickness d (Fig. 1B). When an alternating magnetic field is applied along the axis of the cylinders, it induces a current in the conducting sheet (Fig. 1C). However, although there is no dc path, ac flow is enabled by the self-capacitance of the structure, which completes the resonant circuit. The Swiss roll material is well suited to RF operation because the self-capacitance of the structure is large, and hence the resonant frequency of interaction is within the RF range.

The effective permeability was derived by Pendry *et al.* (*10*) as

$$\mu_{\text{eff}} = 1 - \frac{F}{1 + \dfrac{2\sigma i}{\omega r_0 \mu_0 (N-1)} - \dfrac{d c_0^2}{2\varepsilon \pi^2 r_0^3 (N-1)\omega^2}} \qquad (1)$$

where c_0 is the speed of light in vacuum, ω is the angular frequency, and $i = \sqrt{-1}$. The conductor has a sheet resistance σ, and the insulator between the conductive layers has a permittivity ε. F is the filling factor, the fraction of the material volume that is magnetically active; ideally, this is given as $\pi r_0^2/(2\sqrt{3}a^2)$ where a is the lattice spacing for hexagonal packing, but in practice F is an empirically determined parameter. The resonant frequency of the structure is given by

$$\omega_0 = \sqrt{\frac{d c_0^2}{2\varepsilon \pi^2 r_0^3 (N-1)}} \qquad (2)$$

Our initial Swiss roll structures were constructed using ProFilm Chrome [a proprietary aluminized mylar film, about 50 μm thick, with a thermosetting glue layer (*13*)]. This

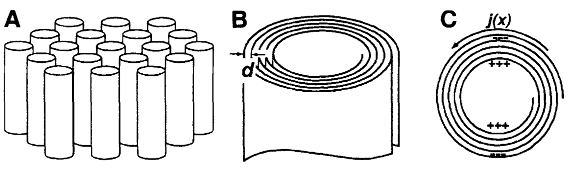

Fig. 1. Schematic diagram of the μSM. **(A)** The material consists of a hexagonal array of 19 cylinders. **(B)** Each cylinder comprises a conducting sheet of thickness *d*, wound on a central mandrel. **(C)** The cross section is a spiral. When a magnetic field parallel to the axis of the cylinder is switched on, it induces a current, *j*(*x*), in the spiral. Distributed capacitance between the turns of the spiral enables current to flow.

[1]Marconi Caswell Ltd., Caswell, Towcester, Northants NN12 8EQ, UK. [2]Imperial College of Science, Technology & Medicine, Prince Consort Road, London SW7 2BZ, UK. [3]Robert Steiner Magnetic Resonance Unit, Clinical Sciences Centre, Imperial College School of Medicine, Hammersmith Hospital, Du Cane Road, London W12 0HS, UK.

*To whom correspondence should be addressed. E-mail: mike.wiltshire@marconi.com

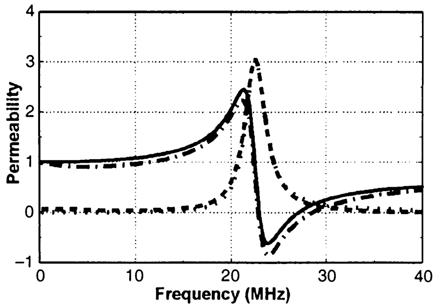

Fig. 2. Measured and calculated permeability for the 35-turn Swiss rolls designed to give a peak in the real part of μ at 21.3 MHz. Here (from top to bottom), the solid line is the calculated real part, the dot-dashed line is the measured real part, the dashed line is the calculated imaginary part, and the dotted line is the measured imaginary part.

material was wound on mandrels made of glass-reinforced plastic (GRP) rod, 200 mm in length. The thickness of the layers obtained when the material had been wound hot was found by direct measurement of the rolls when cold.

RF measurements were made using an HP 4195A Network Analyzer to record the series inductance and resistance as a function of frequency of a solenoid, which was 160 mm long with diameter 60 mm, wound with eight turns of multistrand wire, both when it was empty and with the Swiss roll inserted along its axis. These data were used to obtain the complex permeability ($\mu = \mu' + i\mu''$) by applying corrections for the occupied volume and the demagnetizing field [see, for example, Stratton (*14*)].

The peak frequencies of μ'' were analyzed to provide the effective permittivity, ε, of the ProFilm, and the effective radius of the roll, expressed as $r = r_0 + \alpha dN$, where α is an adjustable parameter to account for the finite thickness of the roll. (The theory in Eq. 1 assumes an infinitesimally thin Swiss roll so that $Nd \ll r_0$, whereas in reality these are comparable.) A least-squares fit to the data provided $\alpha = 0.44$ and $\varepsilon = 3.05$.

The peak widths (full width at half maximum) of μ'' were used to estimate the resistivity of the conducting layer in the ProFilm. We found $\sigma = 1.4$ ohms per square to be the best fitting result, and using the bulk dc resistivity of aluminum (2.65 μohm·cm), we calculated that the corresponding film thickness was ~19 nm. This value is consistent with that measured by scanning electron microscopy.

We then designed a material for use at the 21.3-MHz operating frequency of a Marconi Medical Systems (Cleveland, Ohio) Apollo 0.5-T MRI machine. A GRP mandrel 8 mm in diameter was wound with 35 turns, which theory predicted would give a resonant frequency at 22.1 MHz, with the maximum value of μ' at 21.3 MHz. A set of 19 Swiss rolls, 200 mm long, was made to provide a hexagonal block of material.

These rolls were characterized in various ways, both as individual rods and as bundles of first 7 and then 19 rods. The data obtained are best described in terms of the theory by setting the layer thickness to 49.4 μm and sheet resistance to 1.6 ohms per square; these values are very close to those derived from the initial data. The filling factor F was 0.34, although a much larger value of 0.9 would be expected for a close-packed bundle. The comparison for the bundle of 19 rolls is shown in Fig. 2, from which the excellent agreement between theory and experiment can be seen. The maximum permeability is $\mu = 2.23$ and occurs at 21.23 MHz.

The network analyzer was also used to measure the coupling (S_{21}) between two short coils, linked by a Swiss roll, as a function of their separation. An acetate sleeve was first made, into which a Swiss roll would fit snugly. A five-turn coil was wound 25 mm from one end of this sleeve to act as an RF source. A second five-turn coil was wound on a short movable sleeve to act as a movable detector. Care was taken to ensure that neither the source nor the detector channels were saturated. The coupling between the coils (S_{21}) at 21.3 MHz is plotted in Fig. 3 as a function of the separation of the two coils; the dashed line shows the result without the Swiss roll present. When a 35-turn Swiss roll (which has a maximum in its real part of the permeability at 21.3 MHz) was inserted so that the drive coil was 25 mm from the end of the roll, we obtained the full line. It is clear that the Swiss roll acts as a flux-guiding medium, providing linkage between coils that may be up to 150 mm apart in this case. Note that there is little flux leakage along the length of the core, which is qualitatively different from what would be observed for a conventional magnetic core with a permeability of $\mu \sim 2$.

The properties of this material render it particularly suitable for use in the MRI environment. To demonstrate these characteristics, we used the Swiss rolls as flux guides in an imaging experiment. The layout is sketched in Fig. 4A, which shows the setup used within the bore of a MRI system. The detector coil was a two-turn solenoid with a diameter of 37 mm, tuned to 21.3 MHz. This coil was placed immediately below a water phantom 10 mm thick to provide a reference plane. The object under test (one of the authors' thumbs) was held 200 mm above the water phantom and supported initially on an inert plastic block.

In the MRI machine, low-frequency magnetic field gradients are imposed for short periods upon the large, highly homogeneous main (B_0) field so that during the acquisition of the image data, each point in the field of view (FOV) experiences a unique pattern of magnetic fields. Shaped RF pulses are generated by coils that, in this case, were built into the structure of the main magnet and constitute the "body coils." These pulses, usually in conjunction with an appropriate gradient, excite the nuclei of hydrogen atoms within the desired region, in this case a slice 5 mm thick. After excitation, the nuclei resonate at frequencies corresponding to the ambient field at each point, and further gradient fields are used to provide spatial encoding by making the field a linear function of position. Signals are detected either by the "body coils" (in

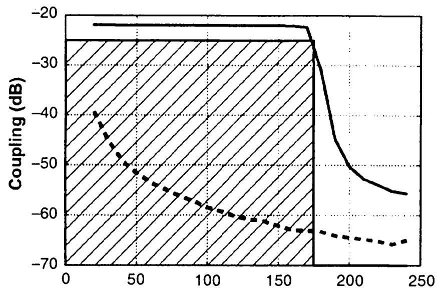

Fig. 3. Measured coupling, S_{21}, as a function of the separation of two coils with a Swiss roll inserted between them (solid line) and with the Swiss roll removed (dashed line). The fixed coil was placed 25 mm from one end of the Swiss roll; the extent of the Swiss roll is indicated by the shading.

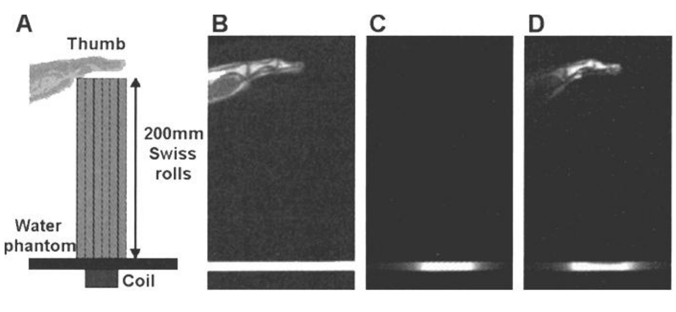

Fig. 4. The MRI imaging experiment. (**A**) Schematic of setup. A small coil (diameter 37 mm) acts as the receiver, and a thumb is the object to be imaged. The water phantom provides a reference plane. The 200-mm space between the phantom and the thumb is filled either with an inert plastic block (not shown) or with Swiss rolls. (**B**) A reference image obtained with the "body coils" that are built into the structure of the magnet. (**C**) The image from the small receiver coil when the thumb is supported on an inert plastic block. Only the phantom is visible. (**D**) The image from the same coil when the Swiss rolls are inserted. Now the image of the thumb can be clearly seen.

transmit-receive mode) or by a separate detector coil or coils. Images are reconstructed from the acquired data by Fourier transformation. Here, sagittal images (i.e., in a vertical plane parallel to the bore of the magnet) were acquired using a standard spin-echo sequence, in which after the exciting pulse a further RF pulse refocuses the signal to form an "echo." Because only part of the data is acquired at any one excitation, the process is repeated and a time period (the repeat time or *TR*) is allowed between excitations to allow for the recovery of the magnetization. In this study, *TR* was 400 ms and the echo time (*TE*) was 15 ms. The FOV was 300 mm by 300 mm with a 256 × 128 data matrix reconstructed to a 256 × 256 image matrix. A single acquisition with no averaging was used in all cases.

The first image (Fig. 4B) was obtained using the "body coil" in transmit-receive mode. This procedure allowed the precise position of the thumb to be determined, so that the subsequent images could be set up accurately. Despite using increased gain, no image could be detected with the small coil alone (Fig. 4C). However, when the bundle of 19 Swiss rolls, 200 mm long, was used to couple the thumb to the receiver coil, a clear image of the thumb was seen (Fig. 4D).

Note that the body coil image (Fig. 4B) allows visualization of the full thumb. This is because the whole of the thumb (and, indeed, beyond) was excited by the RF pulses, and hence was emitting signals. The image obtained by flux guidance through the Swiss rolls is limited by the spatial extent of the flux that could be collected (Fig. 4D). The ratio of the signal measured in a region of the thumb located centrally (10 mm above the free surface of the flux guide) to that measured in a similar region of interest placed in air gave a signal-to-noise ratio (SNR) of 32 for the solenoid with Swiss rolls. The precise SNR value achieved is strongly dependent on the details of measurement because of the spatial nonuniformity of the sensitivity pattern, and it is also dependent on the coupling between the flux guides and the receiver coil. Without the Swiss rolls, no signal from the thumb was detectable with the solenoid coil.

The presence of the Swiss rolls introduces negligible distortion of the main field or the field gradients B_0, because the material has a relative permeability close to unity at dc. Nor does it noticeably distort the effect of the RF excitation field B_1. The spin excitation produced by B_1 is determined by its time integral. Because the material is highly anisotropic, it only interacts with B_1, which is a rotating field, over a very small angular range. Even strong interactions result in only slight perturbations in response, provided they only occur over a small fraction of each cycle, as in this case.

We have demonstrated the unique properties of a microstructured magnetic material operating in the RF band. The material offers a range of frequency-specific permeabilities that can differ widely from unity. The material was used here in an MRI machine to guide the RF flux from an object to a remote receiver coil with little flux leakage, although the material itself was not optimal. In effect, the material has potential to change approaches to optimizing the coil filling factor in nuclear magnetic resonance systems in general, and MRI scanners in particular (*15*, *16*). Improved material should allow much better noise performance, and we expect this to have a substantial impact on the RF systems used in MRI equipment. Finally, we note that the characteristics shown in Fig. 2 indicate that there are frequencies at which $\mu = 0$, when the material would act as a screen, and further frequencies where μ is negative, leading to other unique capabilities. Exploiting this class of materials could fundamentally change existing approaches to magnetic resonance imaging and spectroscopy.

References and Notes

1. H. Ghiradella, *Appl. Opt.* **30**, 3492 (1991).
2. E. Yablonovitch, *Phys. Rev. Lett.* **58**, 2059 (1987).
3. S. John, *Phys. Rev. Lett.* **59**, 2486 (1987).
4. K. M. Ho, C. T. Chan, C. M. Soukoulis, *Phys. Rev. Lett.* **65**, 3152 (1990).
5. E. Yablonovitch, T. J. Gmitter, K. M. Leung, *Phys. Rev. Lett.* **67**, 2295 (1991).
6. D. F. Sievenpiper, M. E. Sickmiller, E. Yablonovitch, *Phys. Rev. Lett.* **76**, 2480 (1996).
7. J. B. Pendry, A. J. Holden, W. J. Stewart, I. Youngs, *Phys. Rev. Lett.* **76**, 4773 (1996).
8. J. B. Pendry, A. J. Holden, D. J. Robbins, W. J. Stewart, *J. Phys. Condens. Matter* **10**, 4785 (1998).
9. D. F. Sievenpiper, L. Zhang, R. F. J. Broas, N. G. Alexopolous, E. Yablonovitch, *IEEE Trans. Microwave Theory Tech.* **47**, 2059 (1999).
10. J. B. Pendry, A. J. Holden, D. J. Robbins, W. J. Stewart, *IEEE Trans. Microwave Theory Tech.* **47**, 2075 (1999).
11. D. R. Smith, W. J. Padilla, D. C. Vier, S. C. Nemat-Nasser, S. Schultz, *Phys. Rev. Lett.* **84**, 4184 (2000).
12. V. G. Veselago, *Sov. Phys. Uspekhi* **10**, 509 (1968).
13. ProFilm material (otherwise known as Oracover) is manufactured by Lanitz-Prena Folien Factory GmbH, Leipzig, and distributed by J. Perkins Distributors Ltd., London.
14. J. A. Stratton, *Electromagnetic Theory* (McGraw-Hill, New York, 1941), pp. 211–214.
15. D. I. Hoult, R. E. Richards, *J. Magn. Reson.* **24**, 71 (1976).
16. D. I. Hoult, P. C. Lauterbur, *J. Magn. Reson.* **34**, 425 (1979).

17. I.R.Y., D.J.L., D.J.G., and J.V.H. are grateful to Marconi Medical Systems for substantial financial support of the work at the Robert Steiner Magnetic Resonance Unit.

16 October 2000; accepted 20 December 2000

Functional Nanoscale Electronic Devices Assembled Using Silicon Nanowire Building Blocks

Yi Cui[1] and Charles M. Lieber[1,2*]

Because semiconductor nanowires can transport electrons and holes, they could function as building blocks for nanoscale electronics assembled without the need for complex and costly fabrication facilities. Boron- and phosphorous-doped silicon nanowires were used as building blocks to assemble three types of semiconductor nanodevices. Passive diode structures consisting of crossed *p*- and *n*-type nanowires exhibit rectifying transport similar to planar *p-n* junctions. Active bipolar transistors, consisting of heavily and lightly *n*-doped nanowires crossing a common *p*-type wire base, exhibit common base and emitter current gains as large as 0.94 and 16, respectively. In addition, *p*- and *n*-type nanowires have been used to assemble complementary inverter-like structures. The facile assembly of key electronic device elements from well-defined nanoscale building blocks may represent a step toward a "bottom-up" paradigm for electronics manufacturing.

Miniaturization of silicon electronics is being intensely pursued (*1*), although fundamental limits of lithography may prevent current techniques from reaching the deep nanometer regime for highly integrated devices (*2*). The use of nanoscale structures as building blocks for self-assembled (*3*–*6*) structures could potentially eliminate conventional and costly fabrication lines, while still maintaining some concepts that have proven successful in microelectronics. One-dimensional structures, such as nanowires (NWs) and carbon nanotubes (NTs), could be ideal building blocks for nanoelectronics (*7*, *8*), because they can

[1]Department of Chemistry and Chemical Biology and [2]Division of Engineering and Applied Sciences, Harvard University, Cambridge, MA 02138, USA.

*To whom correspondence should be addressed. E-mail: cml@cmliris.harvard.edu